

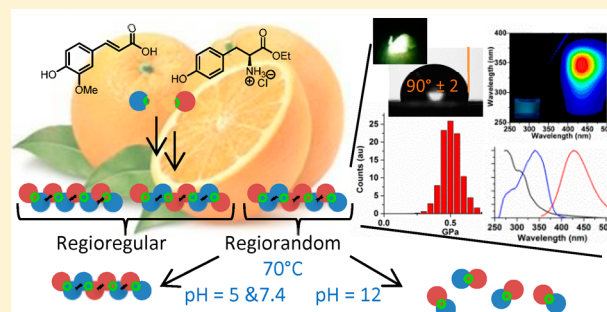
Poly(ferulic acid-co-tyrosine): Effect of the Regiochemistry on the Photophysical and Physical Properties en Route to Biomedical Applications

Amandine Noel, Yannick P. Borguet, Jeffery E. Raymond, and Karen L. Wooley*

Departments of Chemistry, Chemical Engineering, Materials Science and the Laboratory for Synthetic-Biologic Interactions, Texas A&M University, College Station, Texas 77842-3012, United States

S Supporting Information

ABSTRACT: The photophysical and mechanical properties of novel poly(carbonate-amide)s derived from two biorenewable resources, ferulic acid (FA) and L-tyrosine ethyl ester, were evaluated in detail. From these two bio-based precursors, a series of four monomers were generated (having amide and/or carbonate coupling units with remaining functionalities to allow for carbonate formation) and transformed to a series of four poly(carbonate-amide)s. The simplest monomer, which was biphenolic and was obtained in a single amidation synthetic step, displayed bright, visible fluorescence that was twice brighter than FA. Multidimensional fluorescence spectroscopy of the polymers in solution highlighted the strong influence that regioselectivity and the degree of polymerization have on their photophysical properties. The regiochemistry of the system had little effect on the wettability, surface free energy, and Young's modulus (ca. 2.5 GPa) in the solid state. Confocal imaging of solvent-cast films of each polymer revealed microscopically flat surfaces with fluorescent emission deep into the visible region. Fortunately, one of the two regiorandom polymers (obtainable from the biphenolic monomer in only an overall two synthetic steps from FA and L-tyrosine ethyl ester) displayed the most promising fluorescent properties both in the solid state and in solution, allowing for the possibility of translating this system as a self-reporting or imaging agent in future applications. To further evaluate the potential of this polymer as a biodegradable material, hydrolytic degradation studies at different pH values and temperatures were investigated. Additionally, the antioxidant properties of the degradation products of this polymer were compared with its biphenolic monomer and FA.



INTRODUCTION

Multifunctional polymers are often designed and tuned regarding their composition and structure using well-defined chemistry to reach desirable properties for biological and biomedical applications.¹ As such, they are currently developed to solve many urgent issues in the areas of human and environmental health. More specifically, fluorescent labeling for imaging purposes has been extensively investigated for the analysis of biomolecules, determination of biological processes, and evaluation of diseases and therapeutic efficacy.² Consequently, fluorescent polymers may find biomedical applications in domains such as drug delivery, tissue engineering, or as medical devices. Fluorescent properties in these systems are often achieved through conjugation to organic dyes^{3–5} or quantum dots.^{6,7} However, the latter are often toxic,⁸ and organic dyes usually possess low photobleaching resistance.² Often, these agents result in low or unknown contrast agent-to-particle conjugation ratios.⁹ Another approach consists of encapsulating an imaging agent within drug delivery carriers to obtain theranostic nanomaterials; this approach results in changes in size, stability, and complexity of the system. These issues may be circumvented by using label-free polymers

monitored by Raman scattering microscopy,^{10–12} optical coherence tomography,¹³ or alternate fluorescence strategies using, e.g., a dye incorporated directly into the polymer structure.¹⁴ Examples in the literature of autoluminescent polymers used for imaging, targeting, and drug delivery toward breast cancer applications include photoluminescent polyacrylonitrile nanoparticles¹⁵ and multifunctional self-fluorescent polymer nanogels derived from abietane,¹⁶ a bio-based resource. Recently, a label-free fluorescent sensor has been developed based upon the off-on probe principle of the well-known fluorescent poly(2,5-bis(3-sulfonatopropoxy)-1,4-phenylene-*alt*-1,4-poly(phenylene ethylene)) (PPESO₃) for the detection of adenosine triphosphate and alkaline phosphatase in human serum.¹⁷

In order to be used for *in vivo* studies while minimizing cytotoxicity, fluorescent polymers must also be cleared from the body within a reasonable time frame after completing their function. The introduction of biodegradable functionalities can

Received: July 29, 2014

Revised: September 22, 2014

Published: October 14, 2014

increase the difficulty to synthesize and analyze these systems. For example, when labeled with dyes or contrast agents, particularly if polymer degradation rate is fast, biodegradable materials require the application of multiple techniques to determine the extent of coupling.⁹ Moreover, some of the methods applicable to nondegradable polymers/nanoparticles, such as gel electrophoresis, are inappropriate for degradable systems because degradation can be triggered during analysis or sample preparation. Consequently, more precautions are required when handling biodegradable materials, and the assessment of these materials needs to be conducted with a holistic approach. These concerns have led to a desire for readily available, easily translatable, biocompatible, and biodegradable fluorescent materials. One such material was reported by Yang and co-workers as an alternative to existing methods, whereby aliphatic emissive subunits are intrinsic components of the polymer architecture.¹⁸ With this strategy as a guide, we explored in detail the photophysical properties of a new family of poly(carbonate-amide)s¹⁹ and have found that they exhibit remarkable properties, in addition to being derived from natural products through a few synthetic steps. The relationships between the regiochemistry and the photophysical, nanomechanical, and solid state properties of these novel systems were also investigated. The most promising of these materials was further evaluated in terms of its degradability and the antioxidant efficiency of the degradation products released.

EXPERIMENTAL SECTION

Materials. All chemicals and reagents were used as received from Sigma-Aldrich Co. or VWR International. Analytical grade solvents were used for fluorescence analysis. *Caution: special precautions should be taken when working with phosgene precursors, including diphosgene. They are highly toxic by inhalation and ingestion; use of personal protective equipment, including a respiratory mask, is recommended.*

Characterization. ¹H and ¹³C NMR spectra were recorded on a Varian Inova 500 spectrometer. Chemical shifts were referenced to the solvent resonance signals. IR spectra were recorded on a Shimadzu IR Prestige attenuated total reflectance Fourier-transform infrared spectrophotometer (ATR-FTIR) and analyzed using IRSolution v. 1.40 software. Size exclusion chromatography (SEC) measurements were performed on a Waters Chromatography, Inc. (Milford, MA), system equipped with an isocratic pump model 1515, a differential refractometer model 2414, and a four-column set of 5 μm Guard (50 × 7.5 mm), Styragel HR 4.5 μm DMF (300 × 7.5 mm), Styragel HR 4E 5 μm DMF (300 × 7.5 mm), and Styragel HR 2.5 μm DMF (300 × 7.5 mm) using DMF (0.05 M LiBr) as the eluent (1.00 mL/min) at 70 °C. Polymer solutions were prepared at a concentration of ca. 5 mg/mL, and an injection volume of 200 μL was used. Data collection and analysis were performed with Empower 2 v. 6.10.01.00 software (Waters, Inc.). The system was calibrated with poly(ethylene oxide) standards (Polymer Laboratories, Amherst, MA) ranging from 106 to 174 000 Da, and an additional internal calibration based on the oligomeric fraction was also realized.¹⁸ Glass transition temperatures (T_g) were measured by differential scanning calorimetry (DSC) on a Mettler-Toledo DSC822 (Mettler-Toledo, Inc., Columbus, OH) under N₂, as the midpoint of the inflection tangent, upon the third heating scan. Measurements of T_g were recorded with a heating rate of 15 °C/min. The measurements were analyzed using Mettler-Toledo Star^e v.10.00 software. Thermogravimetric analysis (TGA) was performed under an Ar atmosphere using a Mettler-Toledo model TGA/DSC 1, with a heating rate of 10 °C/min. The first-derivative TGA peak (T_p) was evaluated for each compound.

Steady-State Optical Spectroscopy. UV-vis measurements were acquired on a Shimadzu UV-2550 spectrophotometer. All steady-state emission, excitation, and 3D spectra were obtained with a

Horiba FluoroMax4 with automatic polarizer. Measurements were performed in DMF or cyclohexane (specified) in matched quartz cuvettes with path lengths of 2 mm. The measurements are reported in arbitrary units (au).

Lifetime Spectroscopy. Solution-based fluorescence lifetime spectra were obtained using time-correlated single-proton counting (TCSPC). The measurements were done with Fluorotime 100 fluorometer and a 405 nm solid state picosecond diode laser source (PicoQuant) in matched quartz 0.7 mL cells (Starna Cell). Instrument response functions (IRF) were determined from scatter signal solution of Ludox HS-40 colloidal silica (0.01% particules in water S3 w/w). All emission was collected after passing through a 450–520 nm band-pass filter, with a vertical polarizer applied to the excitations source and a magic angle polarizer applied to collection.

Fluorescence Lifetime Microscopy. Fluorescence lifetime imaging was performed using a FLIM LSM upgrade kit (PicoQuant) mounted on a FV1000 (Olympus) confocal microscope with an IX-81 inverted base (Olympus). A 10× dry objective (Olympus) was used for all imaging. The FV1000 system was driven with the FV10-ASW v3.1a software platform (Olympus) with scan rates of 4 μs/pixel at 256 by 256 pixels. FLIM images and TCSPC spectra were collected using bins of 16 ps with 405 nm laser excitation (LDH-P-C-405B, PicoQuant) driven at 20 MHz. The fwhm for the 405 nm laser head was 59 ps, and maximum power was 0.21 mW (attenuated by variable neutral density filters to prevent count pileup and maintain counting rates below 1% bin occupancy).

Atomic Force Microscopy and Surface Force Spectral Mapping. A Bruker Multimode 8 system in PeakForce tapping mode permitted to perform modulus mapping and topographic²⁰ via atomic force microscopy (AFM) measurements. As described previously,²¹ the reduced Young's modulus is directly extracted using the PeakForce QNM imaging mode based on a modified Hertzian model (i.e., the DMT model, which takes into account the surface–tip interactions neglected in the Hertz model). In this study, the system was calibrated using sapphire and then PS standard (modulus = 2.7 GPa). Thermal tuning of the silicon cantilever (k = 48 N/m, VistaProbe) possesses a frequency of 190 kHz with an average deformation of approximately 3 nm. A Poisson ratio of 0.35 was chosen, leading to a potential systemic error for the moduli evaluation of −12% to +8%. All films were formed by solution casting, at the same time, under the same conditions. Polymers were solubilized in warm DMF; a drop was placed on a glass surface. The samples were warmed at 120 °C for 18 h under vacuum, then allowed to cool to room temperature, and heated again to 110 °C for 2 h. After cooling to room temperature, the vacuum was stopped. Films were kept over P₂O₅ under vacuum.

Contact Angle and Surface Free Energy Measurements. Contact angles were measured as static contact angles with an Attension Theta optical tensiometer (Biolin Scientific). The Theta software (Biolin Scientific) calculated the static contact angle using the Young–Laplace formula to fit drops of solvent (water and/or diiodomethane). The reported values correspond to an average as reported in the Supporting Information, Table S5. Surface free energies were also measured using an Attension Theta optical tensiometer (Biolin Scientific). They were calculated through the geometric mean (Owens, Wendt, and Fowkes' equations). With this approach, the surface energy was divided into two components (dispersive and polar). Their contribution was evaluated by the geometric mean approach.

Wide-Field Microscopy. Fluorescence microscopy was performed on an Olympus IX70 inverted microscope equipped with a mercury arc lamp and an Olympus DP72 digital camera. A 10× objective (Olympus UPlanFl n 10×/NA 0.30) was used to collect images. Excitation and S4 emission collection was achieved with the use of an Olympus U-MNIBA3 filter cube with an excitation at 405 nm and an emission between 430 and 530 nm. The optics set, collection time, and CCD gain were kept unchanged for consistency in the measurements.

Pellet Formation. Pellets were formed using a high-pressure hydraulic press (PW225C-XC-9 Bench Press from Phi) heated at 130 °C. About 15 mg of polymer was heated in a homemade mold at 130

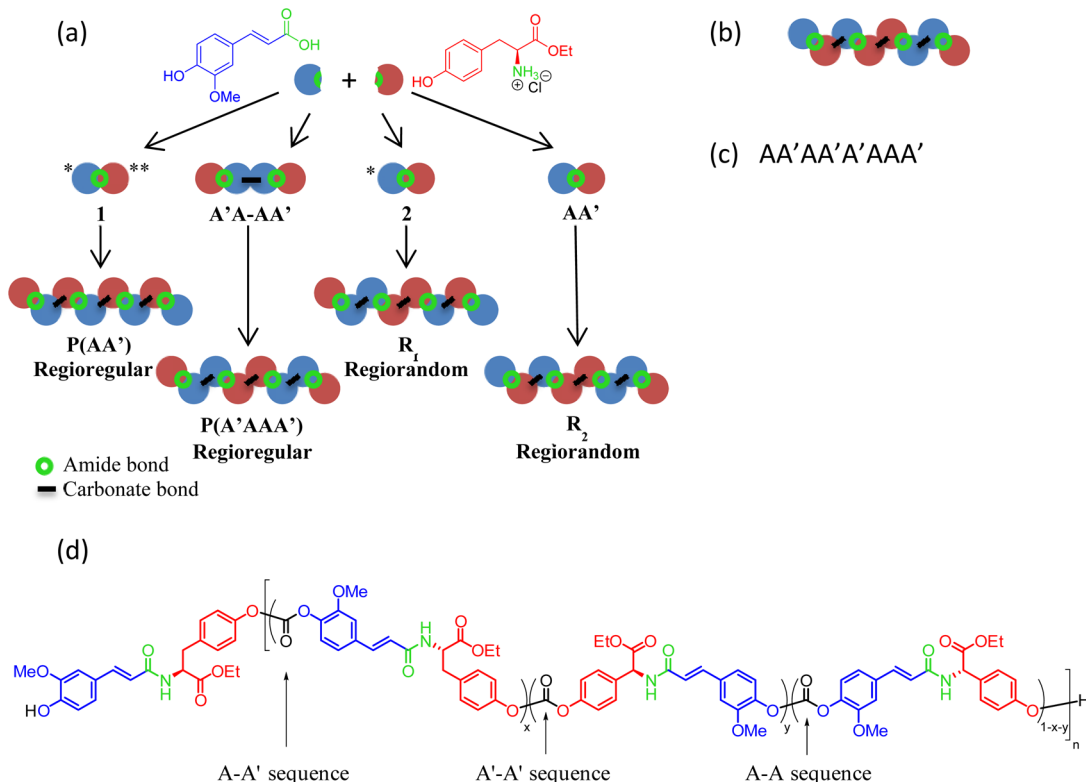


Figure 1. Schematic representations of the monomers and polymers obtained from FA (blue circle) and L-tyrosine ethyl ester (red circle); the amide and carbonate linkages are represented by the green circles and the black lines, respectively. Some monomers were activated (denoted by *) and/or protected (denoted by **) on their phenol groups prior to polymerization (a); schematic representations of a regiorandom polymer with blue, red, and green circles and with the A and A' letters (c); and finally its color-coded chemical structure (d).

°C for 20 min under a pressure of 12 psi generating circular pellets of 4 mm of diameter by 2 mm high. Each pellet had a final weight between 11.0 and 16.1 mg. This difference of mass was taken into account in the analysis.

Radical Scavenging (Antioxidant) Activity. Methanol ACS grade (EMD) was used as the solvent after being stirred on neutral alumina for 48 h and filtered. The antioxidant activity was determined using the radical scavenging activity assay with 2,2-diphenyl-1-picrylhydrazyl radical (DPPH[•]). The linearity and stability of methanolic solutions of DPPH[•] were first confirmed, and then the reaction time necessary to reach the steady state was determined as described in the Supporting Information. The antioxidant activity for FA, monomer AA', and compound 3 was determined by adding 100 μ L of a sample solution (4.95×10^{-4} M) to a 2×10^{-4} M DPPH[•] solution in methanol (3.9 mL). The reaction was stirred at room temperature for 90 min in the dark and analyzed by UV-vis. Experiments were realized in triplicate for each compound. The radical scavenging activity, I , was determined as follows: $I\% = [(\text{Abs}_0 - \text{Abs}_1)/\text{Abs}_0] \times 100$, where Abs_0 was the absorbance at 517 nm of the blank (determined by adding 0.1 mL of methanol to the 3.9 mL of methanolic solutions of DPPH[•]) and Abs_1 was the absorbance at 517 nm in the presence of the test compound. Finally, Welch's t test was used to determine the significance of the difference between the analyzed compounds.

RESULTS AND DISCUSSION

We have recently described the synthesis of bio-based poly(carbonate–amide)s derived from ferulic acid (FA) and L-tyrosine ethyl ester.¹⁹ Those two naturally occurring compounds possess interesting fluorescent properties, and four monomers were designed (Figure 1), allowing for the synthesis of polymers possessing, in some cases, controlled regiochemistries upon polycondensation (Supporting Informa-

tion, Scheme S1). The polymers had previously been fully characterized by NMR spectroscopy and standard thermal analysis. The proportions of each particular regiochemistry, head-to-tail (A–A'), head-to-head (A–A), and tail-to-tail (A'–A'), present in the different polymers had also been determined by thorough analysis of the ¹³C NMR spectra, which enabled us to conduct the current studies to determine the direct effects of the regioregularity on the photophysical and physical properties of the various systems in solution and in the solid state.

The overall goal of this work was to evaluate the impact of the regiochemistry of the poly(ferulic acid-*co*-tyrosine) materials on the physical properties of the systems. Polymers P(AA') and P(A'AAA') were designed to be regioregular and possess either a high amount (90%) or no (~0%) A–A' sequences, respectively. Two regiorandom polymers (R₁ and R₂, from 2 and monomer AA', respectively), containing mainly A–A' sequences (63% and 40%, respectively), were developed to determine the influence of sequence ratios. Finally, the effect of the degree of polymerization (DP) on fluorescence was evaluated through analysis of the regiorandom polymer R₂^S and the regioregular polymer P^S(A'AAA') (Supporting Information, Table S1) (where superscript S stands for short). We first studied the behavior of the polymers in solution, from which it was determined that the regiorandom polymer R₂ was the most fluorescent. Initial solid-state analysis revealed that typical thermal and physical properties remained unaffected by changes in the regioselectivity; however, a more thorough assessment of the fluorescent properties of these materials in the solid state revealed an effect of the regioselectivity on the photophysical properties. Because of its straightforward synthesis and promising fluorescent properties, both in solution

and in the solid state, polymer R_2 was selected as the strongest contender for future applications and was characterized further via determination of its quantum yield. We then investigated the hydrolytic degradability/stability, the nature of the degradation product, and its antioxidant properties, which may define the types of future applications appropriate for R_2 .

Photophysical Properties of the Monomers and Polymers in Solution. Because of their fluorescent properties, FA and tyrosine have found numerous applications as probes for assessing intermolecular interactions in biological media.^{22,23} For example, the interaction of trypsin with FA has been evaluated through several techniques, allowing for the determination of the distance between donor (i.e., trypsin) and acceptor (i.e., FA) as well as the nature of this interaction. Additional applications include the quantification and distribution of FA in food²⁴ as well as the use of three-dimensional emission spectroscopy to differentiate tyrosine from tryptophan in deep-sea chemistry analysis.²⁵

To begin with, we evaluated whether the monomers (monomer AA' and dimer A'A-AA') exhibited higher fluorescence emission intensities than the starting materials (*L*-tyrosine ethyl ester and FA) by using steady-state UV-vis and fluorescence spectroscopies in analytical grade DMF at a concentration of 2.6×10^{-5} M. Multidimensional excitation/emission spectroscopy (3D fluorescence) was used to generate easily interpretable “fingerprints” of the electronic levels of the compounds under investigation. While giving access to information that is similar to that provided by individual spectra (displayed Figure S2, Supporting Information), 3D fluorescence greatly facilitates the visual analysis of the results, especially for compounds possessing slightly different emission/excitation properties, as presented in this work. The use of 3D fluorescence spectroscopy revealed a similar band structure for monomer AA' ($\lambda_{\text{em,max}}$ 387 and 394 nm, $\lambda_{\text{ex,max}}$ 289 and 320 nm) and FA ($\lambda_{\text{em,max}}$ 399 nm and $\lambda_{\text{ex,max}}$ 324 nm) (Figure 2).

An isolated *L*-tyrosine ethyl ester signal was not clearly seen in either the 3D spectrum of monomer AA' or its emission spectrum. The weak signal observed at $\lambda_{\text{ex}} 280$ nm, $\lambda_{\text{em}} 300$ nm that seems to be characteristic of *L*-tyrosine ethyl ester was indeed also present in the 3D spectra of pure FA (Figures 2 and

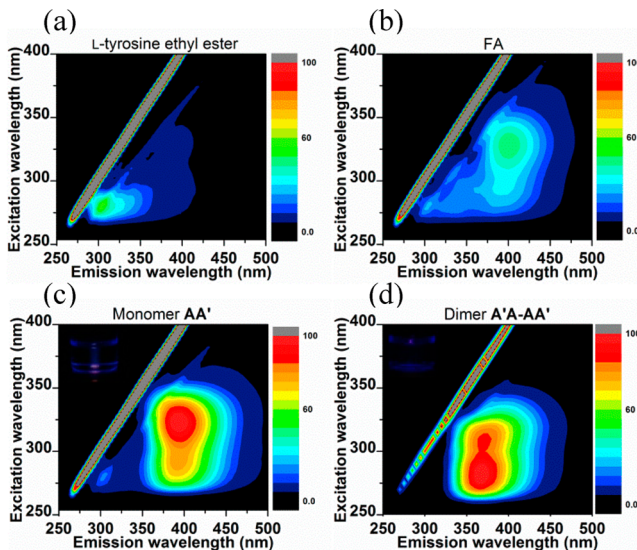


Figure 2. 3D spectra at a concentration of 2.6×10^{-5} M of *L*-tyrosine ethyl ester (a), FA (b), monomer AA' (c), and dimer A'A-AA' (d).

3a). This behavior potentially indicates that Förster resonance energy transfer (FRET) between the tyrosine and FA fragments

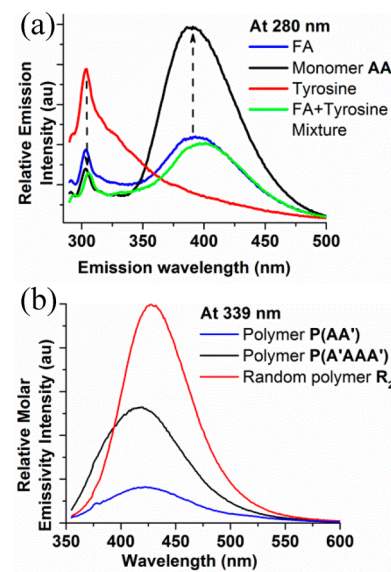


Figure 3. (a) Relative emission intensity of monomer AA', FA, *L*-tyrosine ethyl ester, and a 1:1 mixture of FA:*L*-tyrosine ethyl ester at a concentration of 2.6×10^{-5} M. (b) Relative molar emissivity intensity of polymers P(AA'), P(A'AAA'), and R_2 at 339 nm at a concentration (of the repeat unit) of 5.2×10^{-6} M.

on monomer AA' may be occurring due to the overlap between the emission spectrum of the *L*-tyrosine ethyl ester and the excitation spectrum of FA (Supporting Information, Figure S2). The relative emission intensities of monomer AA' versus FA, *L*-tyrosine ethyl ester, and a 1:1 mixture of *L*-tyrosine ethyl ester and FA were measured to verify this hypothesis (Figure 3a). In the event of a FRET effect, an increase in the relative emission intensity of the acceptor (i.e., FA) would be observed. As no such increase in intensity was observed in the case of the physical blend, proximity alone is insufficient to induce FRET between FA and *L*-tyrosine ethyl ester, resulting instead in the mere quenching of the *L*-tyrosine ethyl ester. Conversely, as also featured in the 3D spectrum, monomer AA' was twice as bright as FA at similar molar concentration, strongly suggesting efficient electronic coupling between the two covalently linked subunits.

The analysis of the 3D spectrum of dimer A'A-AA' revealed that linking two monomers via the phenol groups on the FA residue through a carbonate link (creating an A-A sequence) generates a decrease in the emission intensity at the longer wavelength band (ca. 320 nm ex/395 nm em) and a slightly stronger emission from the shorter wavelength band (ca. 290 nm ex/385 nm em) when compared to monomer AA' (Figure 2d).

After assessment of the various subunits, we then turned our attention toward the resultant polymers. Qualitatively, the regioregular P(A'AAA') and the regiorandom polymers R_2 were the most fluorescent (visually) under a DAPI filter (one of the most common imaging modalities used in microscopy).²⁶ First, 3D fluorescence spectroscopy was used to probe the effects of the regioregularities of the polymers on their photophysical properties (Figure 4; further details can be found in Supporting Information, Figure S3). Comparison of dimer A'A-AA' and its corresponding polymer P(A'AAA')

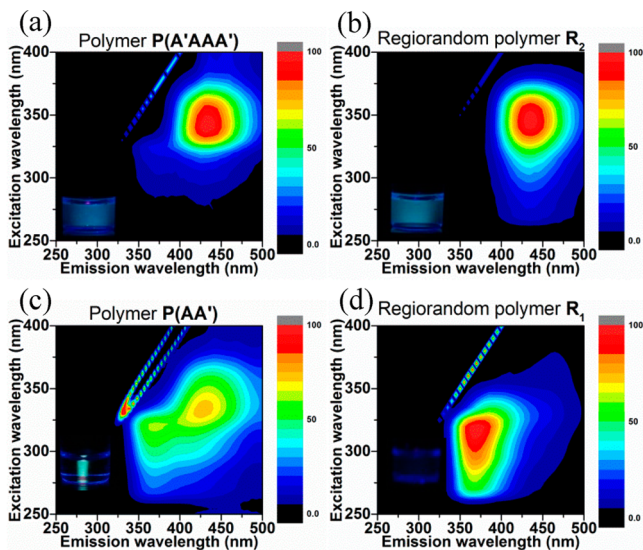


Figure 4. 3D spectra at a concentration (of the repeat unit) of 5.2×10^{-6} M of polymers P(A'AAA') (a), regiorandom R₂ (b), regiorandom R₁ (c), and P(AA') (d). A photo of each polymer imaged under a DAPI filter is presented as an inset with each spectrum.

featured a red-shift in both excitation (289 nm versus 333 nm, respectively) and emission (387 nm versus 415 nm, respectively), placing the emission of P(A'AAA') soundly in the visible spectrum. This fortuitous discovery is particularly useful given the multitude of applications for which biomaterial and medical device fluorescence/contrast is of importance,^{27–29} such as applications where medical staff must rapidly identify biomedical materials during surgery.³⁰ While the formation of an A–A sequence did not appear to affect significantly the fluorescence intensity (monomer AA' versus dimer A'A–AA', *vide supra*), the introduction of A'–A' sequences seemed to enhance fluorescence. The random polymer R₂ possessed a 3D spectrum similar to that of P(A'AAA'). As P(A'AAA') contains as many A–A sequences as A'–A' sequences, it can be deduced that A'–A' sequences dominate the photophysical response of the system over A–A sequence effects (similar to the dimer A'A–AA'). This hypothesis was further supported by the analysis of shorter polymers as discussed in the Supporting Information (Figure S5).

The spectral characteristics of random polymer R₁ (which contained a larger number of A–A' sequences) were comparable to those of dimer A'A–AA', although with a longer λ_{ex} than dimer A'A–AA' (320 and 289 nm, respectively). In order to determine whether the maximum of excitation observed in random polymer R₁ would correlate with its increased A–A' sequences content, steady-state fluorescence spectroscopy of regioregular P(AA') (90% A–A') was investigated. Two emission regimes were observed for P(AA'): a minor emission similar to random polymer R₁ (and possibly attributable to shorter polymer chains) and a primary band at longer wavelengths ($\lambda_{\text{ex}} 339$ nm, $\lambda_{\text{em}} 415$ nm). While the overall emissivity of alternating polymer P(AA') was lower and blue-shifted with respect to polymers P(A'AAA') and random polymer R₂, the dual band structure resulted in a broad-band emitter, with detectable and more uniform emission from <350 to >550 nm. Whether or not this effect can be directly leveraged into biophotonic applications, these findings may be useful in developing blend strategies of

polymers with varied regioselectivity for applications with highly specific spectral needs.

The *ad hoc* determination of relative emission brightness by eye was confirmed by a comparison of the relative molar emissivity intensity of regioregular polymers P(AA'), P(A'AAA') and regiorandom polymer R₂ (Figure 3b). At an excitation wavelength of 339 nm and a concentration (of the repeat unit) of 2.6×10^{-5} M, regiorandom polymer R₂ was 1.9 times brighter than P(A'AAA') and 5.4 times brighter than P(AA').

The combination of the fluorescence investigations described above, along with the knowledge of the polymer topology, as determined by ¹³C NMR spectroscopy, has allowed this partial correlation of the photophysical properties to the regiochemistry. All observed polymers presented broad-band emission spectra in the range of 350–500 nm. Fortunately, this excitation/emission regime corresponds well with common optical systems that are optimized for DAPI fluorescence, a typical organic dye used as a DNA-specific probe and as a biological stain.³¹ An overlay of regiorandom polymer R₂ emission and DAPI emission under similar excitation are presented in the Supporting Information (Figure S6) as well as a summary of the fluorescent properties for all systems investigated (Table S2).

Solid-State Properties. The behaviors of these materials in the solid state were evaluated by a number of methods to afford information about the nanomechanical properties, hydrostatic contact angles, surface free energies, and solid state emission spectra. Each measurement was made with the samples being cast as microscopically thick, uniform films, giving similarities in nanomechanical properties, contact angles, and surface free energies but unique differences in the fluorescence emission characteristics as a function of the polymer regiochemistry. Interestingly, the poly(carbonate-amide)s exhibited mechanical and surface properties comparable to those for poly(bisphenol A) carbonate (BPA PC), while, uniquely, possessing high fluorescence emission intensities.

Homogeneous films of each polymer for nanomechanical mapping of the modulus were obtained by the solvent casting-method from a DMF solution and dried under vacuum at 120 °C. The films presented thicknesses between 45 and 107 μm (Supporting Information, Table S3). Measurements of the moduli were performed in three different locations, and the results are reported as their average values, average point-to-point root-mean-squared variations, and standard deviations (Supporting Information, Table S4). BPA PC ($M_n = 21.4$ kg mol⁻¹), was used as a reference to evaluate the reliability and accuracy of our experimental protocol. A value of 2.2 ± 0.3 GPa was obtained, which is in agreement with the range described in the literature (3.94 GPa³² to 2.3 GPa³³). The four materials presented similar Young's moduli (between 2.6 ± 0.2 and 3.1 ± 0.2 GPa), revealing no influence of the regiochemistry on the nanomechanical properties. Histograms of the compiled data are reported in the Supporting Information (Figure S7). The low variations within the three measurements reveal that surfaces obtained by the solvent-casting method are uniform and that their generation is reproducible.

The homogeneity of all the films was further supported by confocal microscopy of the surfaces, which were flat and uniform at the micro and larger scales (Supporting Information, Figure S8). Despite these similarities, three-color wide field imaging of a 405 nm excitation source qualitatively displayed

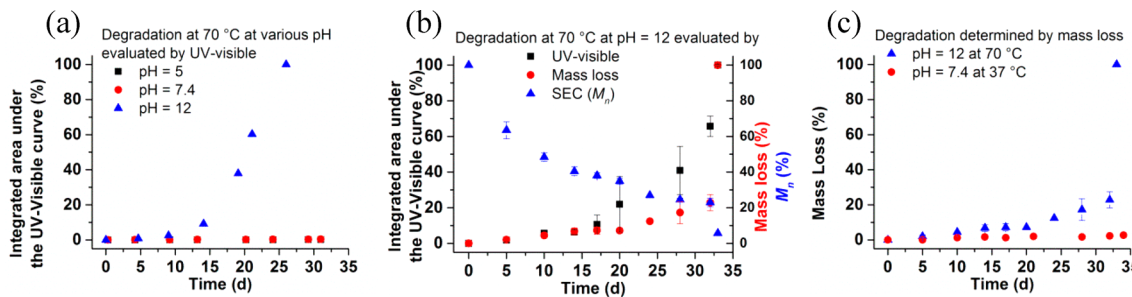


Figure 5. Evaluation of the degradation kinetics of regiorandom polymer \mathbf{R}_2 at various pH values at 70 °C (a), by different methods at pH = 12 at 70 °C (b), and by mass loss at various pH and temperature values (c).

differences in film emission for each sample (Supporting Information, Figures S9 and S10).

All four films presented similar wettability (hydrostatic contact angle ca. 90°, Figure S11 and Table S5) and an average surface free energy (SFE) of ca. 40 mN m⁻¹, as determined by contact angle measurements. These materials, thus, possess a medium to low SFE and contact angles in the same range as bisphenol A polycarbonate (BPA PC), for which the water contact angle is reported to be 92°, as measured by the sessile drop method at 24 °C,^{34,35} and 85 ± 3° by solvent-casting in our hands (SFE of 47.3 ± 0.3 mN m⁻¹). According to these results, these materials might be considered as moderately hydrophobic. In summary, regioregularity appeared to have no significant influence on the contact angle, the SFE, the Young's moduli, or surface roughness of the bulk materials.

To fully evaluate the potential of these materials for biomedical applications (such as contrast, self-reporting, or sensing agents), solid state emission spectra and solid state emission lifetimes have been measured. Under excitation at 405 nm, regiorandom polymer \mathbf{R}_2 and regioregular polymer P(AA') presented the longest emission wavelength maxima (506 nm, 548 nm shoulder and 522 nm, 548 nm shoulder, respectively) (Figure S12). These emission spectra were all red-shifted, in comparison to the solution state (Supporting Information, Table S2). Consequently, in their solid forms, all of the materials emitted far into the visible spectrum, making them good candidates for use in biophotonic applications. As expected, the longest emission wavelength correlated well to the shortest emission lifetimes, evaluated to be ca. 3 ns and shorter (Figure S12b). Of note, all of the species were differentiable in the time domain, in both solution and solid state, perhaps allowing for *in situ* monitoring of the regioselectivity during polymerization. Emission intensity profiles, as determined by confocal microscopy under identical excitation and collection regimes, indicated that both polymers P(A'AAA') and \mathbf{R}_2 were ca. 1 order of magnitude brighter than either polymer P(AA') or \mathbf{R}_1 (Supporting Information, Figure S13). Because of its straightforward, reliable, and high yield synthesis along with its fluorescent properties, random polymer \mathbf{R}_2 appears as a strong contestant for the development of future applications.

Quantum Yield Determination of Regiorandom Polymer \mathbf{R}_2 . Because of its higher emissivity in solution, brightness in the solid state, and its straightforward synthesis, regiorandom polymer \mathbf{R}_2 was chosen to be assessed further with a formal solution state quantum yield study. The quantum yield (Φ) of random polymer \mathbf{R}_2 was determined to be ca. 6%, using 9,10-diphenylanthracene as a standard (see details in Supporting Information as well as an evaluation of the quantum

yield for the other materials). While not in the same league as quantum dots, coumarin, or FITC derivatives, it is still an impressive value considering that (1) the system is bioderived, (2) it shows promise as an engineering biomaterial, (3) it presents a low amount of self-quenching, if any, and (4) there is no need for dye labeling. The quantum yield of polymer 7 in DMF was actually 1.4 times higher than that of DAPI (in water), and the fluorescence lifetime in solution was 10 times longer (2.4 ns for random polymer \mathbf{R}_2 versus 0.2 ns for DAPI).³⁶ Furthermore, organic dyes are usually loaded at a low concentration, while our fluorescent polymers constitute the entirety of the system and consequently can be brighter than dyes incorporated at low percentages.

Degradation Study of Regiorandom Polymer \mathbf{R}_2 and Determination of the Degradation Products.

To complete the characterization of regiorandom polymer \mathbf{R}_2 , hydrolytic degradation studies were conducted under various pH and temperature conditions. In order to be able to observe degradation over a reasonable amount of time (ca. 1 month) and determine the nature of the degradation products, harsher conditions (70 °C) than the ones commonly reported to mimic biological environment were initially selected. In addition to the usual mass loss and molecular weight loss determination of the systems,^{37–39} the degradation was further evaluated through UV-vis spectroscopy, with reliance on the photophysical properties of the water-soluble degradation products. Preliminary experiments performed at 70 °C, over a month, revealed the stability of regiorandom polymer \mathbf{R}_2 under both acidic and neutral pH values (pH = 5 and 7.4), while significant degradation occurred after only 15 days at pH = 12 (Figure 5). Since the degradation experiment performed at pH = 12 and 70 °C was the only one leading to measurable amounts of degradation products, the reaction was repeated in duplicates with monitoring of the mass loss and the M_n of the polymer as a function of time. After 15 days, 10% of the total mass of the pellet was lost, the M_n of the polymer had decreased by ca. 60%, and 10% of the total initial absorbance was observed by UV-vis spectroscopy. Complete degradation, as evidenced by the disintegration of the pellet, occurred within a month. To simulate a biological environment, this experiment was also performed at 37 °C in PBS buffer over an extended period of time. As expected from the preliminary study, no measurable mass loss or absorbance increase was recorded over a 4 month period. A strong effect of the pellet conditioning was observed that may explain the large error bars: while the pellet degraded completely within 26 days at pH = 12 and 70 °C during our preliminary study, 33 days were necessary for the duplicates under identical conditions.

The nature of the major degradation products was identified and confirmed by spectroscopic and spectrometric analyses. Under basic conditions, regiorandom polymer \mathbf{R}_2 was expected to degrade through its carbonate groups (generating CO_2 and the corresponding phenols) as well as through the cleavage of the ester side chain (generating ethanol and the corresponding carboxylic acid). The degradation mixture was analyzed by UV-vis and ^1H NMR spectroscopies and mass spectrometry to determine the nature of the degradation products (Figure 6).

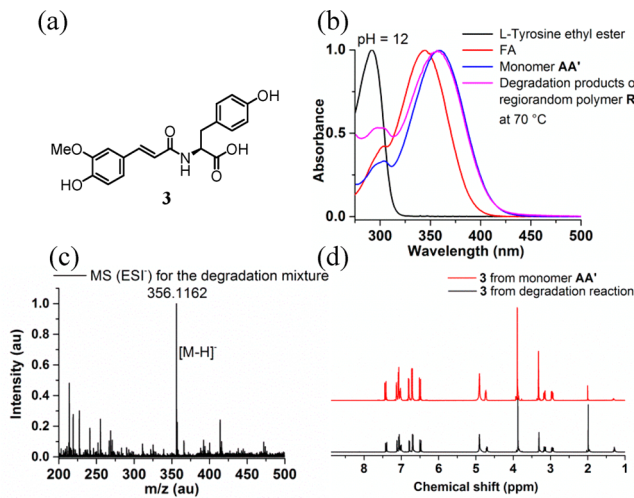


Figure 6. Identification of the degradation product. Chemical structure of the expected degradation product, 3 (a), absorbance spectra of L-tyrosine ethyl ester, FA, monomer AA', and degradation product from regiorandom polymer \mathbf{R}_2 generated at pH = 12 and 70 °C (b), mass spectrometry of the degradation mixture by negative electrospray ionization (c), and ^1H NMR spectra of the expected degradation product 3 and from the degradation mixture of regiorandom polymer \mathbf{R}_2 (d).

The spectral resemblance of the degradation mixture with monomer AA' in contrast to both FA and L-tyrosine ethyl ester indicated the likely structural similarity of monomer AA' and the degradation product. This assumption was unequivocally confirmed by the independent synthesis of the expected degradation product (3, see details in Supporting Information) and comparison of the spectral and spectrometric data. Interestingly, the formation of compound 3 under basic conditions by degradation of regiorandom polymer \mathbf{R}_2 demonstrates the recyclability of this system since the degradation product (3) could then be esterified using standard conditions and further repolymerized to random polymer \mathbf{R}_2 .

Antioxidant Properties of FA, Monomer AA', and Degradation Product 3. The study was completed by comparing the radical scavenging (antioxidant) activity of monomer AA', compound 3, and FA. To do so, the radical scavenging activity assay using 2,2-diphenyl-1-picrylhydrazyl radical (DPPH^\bullet) was used.^{40,41} This purple radical possesses an intense absorption band at 517 nm, which decreases when the radical is quenched. Working at a concentration of 2×10^{-4} M of DPPH^\bullet and 4.95×10^{-4} M of the different samples, the steady state was achieved in approximately 45 min (Figure 7a). Therefore, the antioxidant activity was evaluated in triplicate by reduction of DPPH^\bullet after 1.5 h. Similar activities were observed for all three compounds, although a statistical difference between FA and compound 3 was noticed according to Welch's *t* test (Figure 7b). It is worth mentioning that there is

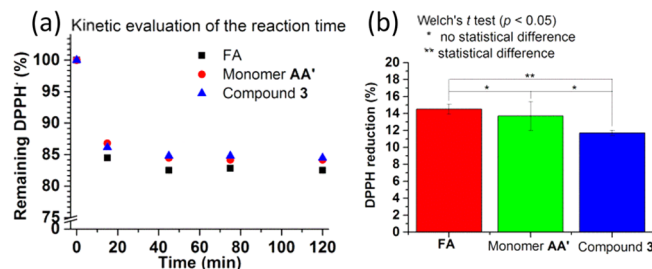


Figure 7. Evaluation of reaction time to reach the steady state (a) and DPPH^\bullet reduction by FA, monomer AA', and compound 3 as well as results of Welch's *t* test (b).

still some debate in the literature as to whether closely related (*E*)-N-(feruloyl)-L-tyrosine methyl ester 4 (Figure S20) is a stronger antioxidant than FA, depending on the methodology used.^{42,43} In our hands, similar activities were observed for monomer AA' and the degradation product 3.

CONCLUSIONS

Our recent report of the synthesis of four new poly(carbonate-amide)s derived from fluorescent bio-based resources¹⁹ led us to investigate their photophysical, nanomechanical, and hydrolytic degradation properties. Steady-state fluorescence spectroscopy (in general) and the 3D spectra (in particular) revealed that monomer AA' presents emissive fluorescent properties similar to FA but twice higher in intensity, attributable to FRET between the L-tyrosine ethyl ester part and the FA part of monomer AA'. Dimer A'A-AA', which presented a 3D spectrum slightly blue-shifted in comparison to monomer AA', was used to generate the regioregular polymer P(A'AAA') (containing only A-A and A'-A' sequences). This polymer possessed a 3D spectrum similar to the regiorandom polymer \mathbf{R}_2 (with a high content of A'-A' sequences). These similarities highlight the strongest impact of A'-A' sequences over A-A sequences on the fluorescent properties.

Nanomechanical studies revealed similar Young's moduli and roughnesses for all these materials (ca. 2.9 GPa), which were also comparable to the behavior of BPA PC. Moreover, regioregularity did not induce any significant differences in the wettabilities and the surface free energies for any of these materials, which were all slightly hydrophobic. Solid-state fluorescence spectroscopy highlighted the potential of regiorandom polymer \mathbf{R}_2 as a biophotonic material. A quantum yield of 6% in DMF was observed for regiorandom polymer \mathbf{R}_2 , which enables us to envisage this polymer as a potential self-reporting or imaging agent.

Finally, degradation studies revealed the stability of regiorandom polymer \mathbf{R}_2 under acidic and neutral conditions, while at pH = 12, a substantial degradation occurred within 15 days releasing compound 3, identified through multispectral analysis and mass spectrometry. The hydrolytic stability of these materials suggests that they may be broadly applicable as (bio)engineering materials for long-term performance, even under extreme conditions, not necessarily with the intention for their degradation.

Regiorandom polymer \mathbf{R}_2 , derived from rather inexpensive bio-based resources in only two steps, can be an alternative to the existing autofluorescent biodegradable systems,¹⁹ depending on the application targeted. Moreover, with the mechanical properties being comparable to BPA PC, it offers advantages of fluorescence activity that may open new applications as a

replacement for a traditional polycarbonate material. Its fluorescent properties in the visible spectrum might be particularly useful given the multitude of applications for which biomaterial and medical device fluorescence/contrast is of importance,^{27–29} such as applications where medical staff must rapidly identify biomedical materials during surgery.³⁰ The synthesis of micelles is currently under investigation in our laboratory to evaluate the potential of this material as a self-reporting drug delivery vehicle.

■ ASSOCIATED CONTENT

Supporting Information

Additional characterization and spectroscopic information. This material is available free of charge via the Internet at <http://pubs.acs.org>.

■ AUTHOR INFORMATION

Corresponding Author

*E-mail: wooley@chem.tamu.edu (K.L.W.).

Notes

The authors declare no competing financial interest.

■ ACKNOWLEDGMENTS

We gratefully acknowledge financial support from the National Science Foundation (CHE-1057441 and CHE-1410272), the National Heart Lung and Blood Institute of the National Institutes of Health as a Program of Excellence in Nanotechnology (HHSN268601000046C), and the Welch Foundation through the W. T. Doherty-Welch Chair in Chemistry (A-0001). We also acknowledge Dr. Hung-Jue Sue and Mr. Kevin Laux for access to their hydraulic press and their kind explanations.

■ ABBREVIATIONS

AFM, atomic force microscopy; ATR-FTIR, attenuated total reflectance–Fourier-transform infrared spectroscopy; BPA PC, poly(bisphenol A) carbonate; DAPI, 4',6-diamidino-2-phenylindole; DMF, *N,N*-dimethylformamide; DMT, Derjaugin, Muller, and Toporov; DNA, deoxyribonucleic acid; DP, degree of polymerization; DPPH, 2,2-diphenyl-1-picrylhydrazyl radical; DSC, differential scanning calorimetry; FA, ferulic acid; FITC, fluorescein isothiocyanate; FLIM LSM, fluorescence-lifetime imaging microscopy laser scanning microscopy; FRET, Förster resonance energy transfer; fwhm, full width at half-maximum; λ_{em} , emission wavelength; λ_{ex} , excitation wavelength; NMR, nuclear magnetic resonance; PS, polystyrene; QNM, quantitative nanomechanical property mapping; SEC, size-extrusion chromatography; SFE, surface free energy; TCSPC, time-correlated single-proton counting; TGA, thermogravimetric analysis; UV-vis, ultraviolet–visible.

■ REFERENCES

- (1) Elsabahy, M.; Wooley, K. L. *Chem. Soc. Rev.* **2012**, *41*, 2545–2561.
- (2) Zhang, Y.; Yang, J. *J. Mater. Chem. B* **2013**, *1*, 132–148.
- (3) Gonil, P.; Sajomsang, W.; Ruktanonchai, U. R.; Na Ubol, P.; Treetong, A.; Opanasopit, P.; Puttipipatkhachorn, S. *Biomacromolecules* **2014**, *15*, 2879–2888.
- (4) Relogio, P.; Bathfield, M.; Haftek-Terreau, Z.; Beija, M.; Favier, A.; Giraud-Panis, M.-J.; D'Agosto, F.; Mandrand, B.; Farinha, J. P. S.; Charreyre, M.-T.; Martinho, J. M. G. *Polym. Chem.* **2013**, *4*, 2968–2981.
- (5) Ma, X.; Wang, Y.; Zhao, T.; Li, Y.; Su, L.-C.; Wang, Z.; Huang, G.; Sumer, B. D.; Gao, J. *J. Am. Chem. Soc.* **2014**, *136*, 11085–11092.
- (6) Wu, P.-J.; Ou, K.-L.; Chen, J.-K.; Fang, H.-P.; Tzing, S.-H.; Lin, W.-X.; Chang, J.-Y. *Mater. Lett.* **2014**, *128*, 412–416.
- (7) Shen, L. *J. Funct. Biomater.* **2011**, *2*, 355–372.
- (8) Ghaderi, S.; Ramesh, B.; Seifalian, A. M. *J. Drug Targeting* **2011**, *19*, 475–486.
- (9) Gustafson, T. P.; Lim, Y. H.; Flores, J. A.; Heo, G. S.; Zhang, F.; Zhang, S.; Samarajeewa, S.; Raymond, J. E.; Wooley, K. L. *Langmuir* **2014**, *30*, 631–641.
- (10) Lui, Z.; Tabakman, S.; Dai, H. *Nano Res.* **2009**, *2*, 85–120.
- (11) Freudiger, C. W.; Min, W.; Saar, B. G.; Lu, S.; Holtom, G. R.; He, C.; Tsai, J. C.; Kang, J. X.; Xie, X. S. *Science* **2008**, *322*, 1857–1860.
- (12) Chernenko, T.; Matthäus, C.; Milane, L.; Quintero, L.; Amiji, M.; Diem, M. *ACS Nano* **2009**, *3*, 3552–3559.
- (13) Au, K. M.; Lu, Z.; Matcher, S. J.; Armes, S. P. *Biomaterials* **2013**, *34*, 8925–8940.
- (14) Robin, M. P.; Mabire, A. B.; Damborsky, J. C.; Thom, E. S.; Winzer-Serhan, U. H.; Raymond, J. E.; O'Reilly, R. K. *J. Am. Chem. Soc.* **2013**, *135*, 9518–9524.
- (15) Lee, K. J.; Oh, W.-K.; Song, J.; Kim, S.; Lee, J.; Jang, J. *Chem. Commun.* **2010**, *46*, 5229–5231.
- (16) Chen, Y.; Wilbon, P. A.; Zhou, J.; Nagarkatti, M.; Wang, C.; Chu, F.; Tang, C. *Chem. Commun.* **2013**, *49*, 297–299.
- (17) Li, Y.; Li, Y.; Wang, X.; Su, X. *New J. Chem.* **2014**, *38*, 4574–4579.
- (18) Yang, J.; Zhang, Y.; Gautam, S.; Liu, L.; Dey, J.; Chen, W.; Mason, R. P.; Serrano, C. A.; Schug, K. A.; Tang, L. *Proc. Natl. Acad. Sci. U. S. A.* **2009**, *106*, 10086–10091.
- (19) Noel, A.; Borguet, Y. P.; Raymond, J. E.; Wooley, K. L. *Macromolecules* **2014**, *47*, 2974–2983.
- (20) Young, T. J.; Monclus, M. A.; Burnett, T. L.; Broughton, W. R.; Ogin, S. L.; Smith, P. A. *Meas. Sci. Technol.* **2011**, *22*, 125703–125706.
- (21) Imbesi, P. M.; Raymond, J. E.; Tucker, B. S.; Wooley, K. L. *J. Mater. Chem.* **2012**, *22*, 19462–19473.
- (22) Shuai, L.; Chen, Z.; Fei, P.; Wang, Q.; Yang, T. *Luminescence* **2014**, *29*, 79–86.
- (23) Sgarbossa, A.; Lenci, F. *J. Fluoresc.* **2013**, *23*, 561–567.
- (24) Ndolo, V. U.; Beta, T.; Fulcher, R. G. *Food Res. Int.* **2013**, *52*, 109–118.
- (25) Jiang, C.-y.; Yuan, Y.; Sun, Z.-j.; Ye, S.-m.; Chen, H.; Pan, Q.-m. *J. Lumin.* **2013**, *135*, 42–46.
- (26) Corich, V.; Soldati, E.; Giacomini, A. *Ann. Microbiol.* **2004**, *54*, 335–342.
- (27) Corr, S.; Rakovich, Y.; Gun'ko, Y. *Nanoscale Res. Lett.* **2008**, *3*, 87–104.
- (28) Zufferey, J.; Rime, B.; Francioli, P.; Bille, J. *J. Clin. Microbiol.* **1988**, *26*, 175–177.
- (29) Sjollema, J.; Sharma, P. K.; Dijkstra, R. J. B.; van Dam, G. M.; van der Mei, H. C.; Engelsman, A. F.; Busscher, H. J. *Biomaterials* **2010**, *31*, 1984–1995.
- (30) Torbati, A. H.; Mather, R. T.; Reeder, J. E.; Mather, P. T. *J. Biomed. Mater. Res., Part B* **2014**, *102*, 1236–1243.
- (31) Kapuscinski, J. *Biotechnol. Histochim.* **1995**, *70*, 220–233.
- (32) Larsson, A.; Dérand, H. *J. Colloid Interface Sci.* **2002**, *246*, 214–221.
- (33) Feller, J. F.; Bourmaud, A. *Polym. Degrad. Stab.* **2003**, *82*, 99–104.
- (34) Stachewicz, U.; Li, S.; Bilotti, E.; Barber, A. H. *Appl. Phys. Lett.* **2012**, *100*, 094101–094104.
- (35) Lapčík, L., Jr.; Fraštík, M.; Lapčíková, B. *Int. J. Heat Mass Trans.* **2012**, *55*, 1513–1518.
- (36) Härd, T.; Fan, P.; Kearns, D. R. *Photochem. Photobiol.* **1990**, *51*, 77–86.
- (37) Wang, Y.-h.; Shi, Y.-y.; Dai, J.; Yang, J.-h.; Huang, T.; Zhang, N.; Peng, Y.; Wang, Y. *Polym. Int.* **2013**, *62*, 957–965.
- (38) Pêgo, A. P.; Poot, A. A.; Grijpma, D. W.; Feijen, J. *Macromol. Biosci.* **2002**, *2*, 411–419.

- (39) Xiao, C.; Zhu, K. J. *Macromol. Rapid Commun.* **2000**, *21*, 1113–1115.
- (40) Scherer, R.; Godoy, H. T. *Food Chem.* **2009**, *112*, 654–658.
- (41) Brand-Williams, W.; Cuvelier, M. E.; Berset, C. *LWT* **1995**, *28*, 25–30.
- (42) Georgiev, L.; Chochkova, M.; Totseva, I.; Seizova, K.; Marinova, E.; Ivanova, G.; Ninova, M.; Najdenski, H.; Milkova, T. *Med. Chem. Res.* **2013**, *22*, 4173–4182.
- (43) Spasova, M.; Kortenska-Kancheva, V.; Totseva, I.; Ivanova, G.; Georgiev, L.; Milkova, T. *J. Pept. Sci.* **2006**, *12*, 369–375.